IEEE Access
Multidisciplinary | Rapid Review | Open Access Journal

Received 28 August 2023, accepted 20 September 2023, date of publication 25 September 2023,
date of current version 28 September 2023.

Digital Object Identifier 10.1109/ACCESS.2023.3319216

RESEARCH ARTICLE

Dual-Band Two-Port MIMO Antenna for Biomedical Deep Tissue Communication: Design, Characterization, and Performance Analysis

SYED NAZIM SHAH[1], MUHAMMAD ZADA[2], (Graduate Student Member, IEEE), JAMAL NASIR[1], SYED MANAF ALI SHAH[1], EMILIO ARNIERI[3], (Member, IEEE), AND HYOUNGSUK YOO[2,4], (Senior Member, IEEE)

[1]Department of Electrical and Computer Engineering, COMSATS University Islamabad, Abbottabad Campus, Abbottabad 22060, Pakistan
[2]Department of Electronic Engineering, Hanyang University, Seoul 04763, Republic of Korea
[3]Dipartimento di Electtronica, Informatica e Sistemistic, University of Calabria, 87036 Rende, Italy
[4]Department of Biomedical Engineering, Hanyang University, Seoul 04763, Republic of Korea

Corresponding author: Hyoungsuk Yoo (hsyoo@hanyang.ac.kr)

This work was supported in part by the Institute of Information and Communications Technology Planning and Evaluation (IITP) Grant by the Korean Government through the Ministry of Science and ICT (MIST) under Grant 2022-0-00310, and in part by the National Research Foundation of Korea (NRF) Grant by the Korean Government through MSIT under Grant 2022R1A2C2003726.

ABSTRACT The demand for wireless communication in biomedical applications is increasing, thereby necessitating the development of reliable and efficient communication systems that can operate within the human body. This study introduces a novel dual-band two-port multiple-input multiple-output (MIMO) implantable antenna for deep tissue purposes with an overall size of $10.8 \times 5.6 \times 0.254$ mm^3 = 15.3 mm^3. The proposed MIMO antenna operates in the 915 and 2450 MHz industrial scientific medical bands with a measured bandwidth of 82.5, 148.5 MHz (port 1) and 130, 89 MHz (port 2), in addition peak realized gains of −32.15 and −22.2 dBi, respectively, are observed. High-measured port isolation (over 20 dB and 30 dB at 915 and 2450 MHz bands, respectively) was accomplished by means of meandered resonators. The determined specific absorption rate was within the safe limits. The MIMO performance factors, for instance, the envelope correlation coefficient and diversity gain, were also evaluated and determined to be in the acceptable range. According to our knowledge, this is the first dual-band implantable MIMO antenna developed for biomedical applications. The results from the simulations and measurements indicate that the developed antenna holds great promise for enabling effective communication within the human body for biomedical applications.

INDEX TERMS Biomedical applications, diversity gain, envelope correlation coefficient, industrial scientific medical, diversity gain multiple-input multiple-output, specific absorption rate.

I. INTRODUCTION

Recently, the need for implanted medical devices (IMDs) in medical services and diagnostic applications, such as pacemakers, intraoral tongue-drive systems, and intrathoracic pressure monitoring, has significantly increased [1]. This is because IMDs may harvest bio-signal characteristics from numerous human organs and wirelessly transfer the necessary information to the receiving device. Recent advancements have been made in the application of IMDs for cardiac pacemakers [2], brain stimulation and monitoring [3], wireless capsule endoscopies [5], proactive cataract intraocular pressure measurement [6], and glucose monitoring devices [7]. IMDs may have several electronic and RF components, including sensor systems, batteries, filters, and antennas [8]. Hence, in recent years, a substantial focus has been placed on the development of implantable antennas, which are a critical part of IMDs. Kiourti et al. [9] presented comprehensive design standards, testing methodologies, radiation quality standards, and reliable link budget concerns for biomedically implanted antennas. The design of implantable antennas is challenging owing to

The associate editor coordinating the review of this manuscript and approving it for publication was Giorgio Montisci.

size constraints, the complex, and lossy nature of the human body, resulting in antenna properties that differ from those in free space [10]. Various types of implantable antennas, such as quad-band [12], triple-band [13], dual-band [4], single-band [16], and wide-band [18] antennas, were recently suggested to satisfy the requirements of compactness, acceptable radiation, safety, and reliable link performance. However, these designs feature a single-input single-output (SISO) arrangement. SISO antennas cannot meet the demand for spectrum efficiency and high data rates. In addition, these SISO antennas cannot increase the data rates once their bandwidth is defined, and the designs are fabricated [19]. They also suffer from multipath distortion, making them susceptible to signal degradation. The heterogeneous human body environment further affects the performance of implantable antennas regarding channel capacity, owing to harsh channel propagation scenarios caused by multipath propagation of signals from the IMD to the external receiver, resulting from the various dielectric properties of different tissues within the human body. This degrades the performance of the biomedical antennas. The multiple-input multiple-output (MIMO) approach, which employs several antennas on both the transmitting and receiving sides, solves these shortcomings. Recently, MIMO implantable antennas have been recommended to offer increased spectral efficiency [20]. MIMO antenna systems increase the channel capacity compared with SISO antenna systems, without consuming extra bandwidth or power [21]. Therefore, the MIMO technique is suitable for providing high data rates for implantable medical applications. The first multi-input, multi output (MIMO) implanted antenna for wireless-capsule endoscopy application was suggested in [20], comprising two elements operating in the 402-405 MHz frequency band. In [19], a 2.45 GHz MIMO implantable antenna with two elements for deep-tissue implants was presented. The antenna had dimensions of 5.35 × 6.2 × 0.12 mm^3 and achieved the isolation of 28 dB by using vertical gaps in the ground layer. In [22], a low-profile two-section MIMO implantable antenna for capsule endoscopy and scalp implantation applications was proposed, which covers the medical implant communication service (MICS) spectrum of 402×405 MHz, and industrial, scientific, and medical (ISM) band of 433.1×438.8 MHz. The antenna had a size of $\pi \times (5.65)^2 \times 0.13$ mm^3 and an isolation of 26 dB was attained by employing a slotted ground plane. In [23], the authors presented a four-port conformal MIMO antenna functioning at the 915 MHz spectrum for capsule endoscopy. The antenna has a volume of 31.4 × 15 × 0.2 mm^3 and achieved an isolation of 20 dB across the neighboring sections. Similarly, authors in [24] presented a reduced four-element MIMO implantable antenna with a volume of 18.5 × 18.5 × 1.27 mm^3 operating at a 2.45 GHz ISM spectrum. An isolation of 15 dB was attained through the use of electromagnetic bandgap (EBG) layouts in the design. In [25], the authors presented a four-port MIMO antenna for scalp implants functioning in a 433 MHz ISM spectrum. The antenna had dimensions of 13.5 × 13.5× 0.13 mm^3 and offered an isolation of 32 dB. Other works, such as [26], [27], and [28], have also presented MIMO implantable antennas for various single-band biotelemetry applications. All previous MIMO implantable antenna designs only support operation in one frequency band; however, a multiband operation is preferable for multifunctional implantable medical devices that require multiple frequencies for tasks, for instance, wireless charging plus waking up [10]. In addition, external noise sources and RF interfaces can negatively affect wireless communication by reducing the signal-to-noise ratio (SNR). To ensure safety and robustness, having multiple bands rather than just one is advantageous. Thus, if one band is significantly impacted by outside interference, an additional can be used as a backup to maintain system operation [29]. Therefore, the design of a dual-band MIMO implantable antenna is highly desirable.

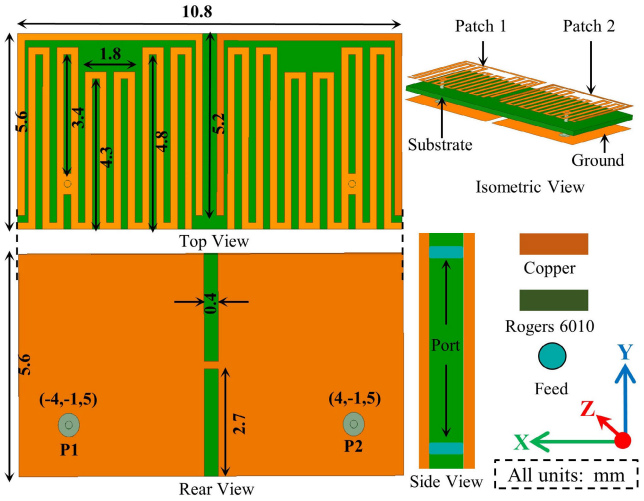

FIGURE 1. Proposed dual-band two-elements MIMO antenna geometry.

This study suggests a compact dual-band two-port MIMO implantable antenna for deep-tissue implantable devices to overcome these problems and ensure safety and robustness. It operates simultaneously at 915 and 2450 MHz bands for multi-tasking biotelemetry applications and interference avoidance. Compactness was achieved using meandered resonators and a slot in the ground plane without shortening pins. Furthermore, to enhance port isolation, no mutual coupling reduction technique was employed. Instead, the meandered lines were strategically designed to counteract the field effects restricting from oppositely flowing currents on adjacent lines of the radiating patch, occurring at both resonances. As a consequence, this approach effectively reduced the electromagnetic flow directed toward the neighboring port, thereby yielding optimum isolation between the ports. The proposed MIMO system was simulated, and measurements were performed on a quasi-implantable device containing sensors, batteries, substrates, and lumped elements. This is, as far as we are aware, the first implantable dual-band MIMO antenna ever proposed.

II. PROPOSED IMPLANTABLE MIMO ANTENNA DESIGN

The top, bottom, and isometric geometry of the suggested antenna is depicted in Figure 1. The proposed antenna is designed to operate at ISM bands of 915 and 2450 MHz. The selection of these frequency bands is due to their technical benefits and practical considerations. These bands fall within the ISM spectrum, offering regulatory advantages and unlicensed communication opportunities. Our motivation lies in utilizing these bands to achieve higher data rates due to their larger bandwidths, as compared to the medical implant communication service (MICS) band of 402 MHz, for real-time biotelemetry applications, where rapid information exchange is critical. Moreover, the 915 MHz band aligns with the need for deep tissue communication, utilizing its larger wavelength to penetrate biological tissues effectively. This minimizes signal loss and attenuation, ensuring robust communication in complex biological environments. The preference for ISM bands is also supported by their broad bandwidth, high data rate capabilities, and compact antenna requirements. The suggested antenna for MIMO is made up of two meandering resonators designed on the upper layer of a Rogers RO6010 substrate ($\varepsilon_r = 10.2$, loss factor (tanδ) = 0.0023 and thickness of 0.254 mm) with dimensions of $10.8 \times 5.6 \times 0.254$ mm^3 = 15.3 mm^3. This ultrathin substrate minimizes mutual coupling between the resonators by suppressing the surface wave propagation [29]. The radiators were supported by a slotted ground layer of the same size as the substrate. The ground slots in the proposed antenna improve element isolation by decreasing coupling and by reducing the passage of current between both feeding ports. The designed antenna was enclosed within a flat-type dummy IMD, as shown in Fig. 2a, to replicate a realistic environment. This IMD includes batteries with perfect electrical conductivity properties, silicon-based electronic components, and a PCB made of Rogers RO6010 ($\varepsilon_r = 10.2$, loss factor (tanδ) = 0.0023, and thickness of 0.254 mm). The dimensions of the IMD are $13 \times 8 \times 3.25$ mm^3 and enclosed in a biocompatible alumina (Al_2O_3) shell with ε_r = 9.8, loss factor (tanδ) = 0.006, and thickness of 0.2 mm. The suggested MIMO antenna combined with a flat device was simulated and optimized using the HFSS software in a frequency-dependent heterogeneous muscle phantom with dimensions of $100 \times 100 \times 100$ mm^3 and a depth of 58 mm. The phantoms were surrounded by a radiation boundary of $300 \times 300 \times 300$ mm^3, as illustrated in Fig. 2a. The frequency dependence of tissue properties poses a challenge for the design of multi-band implantable antennas, which is addressed by considering them to be frequency-dependent in the desired range of 0.5-3 GHz. Further evaluation was conducted using the Remcom simulator by implanting the suggested MIMO antenna system in a human Duke model, as shown in Fig. 2a. A prototype of the suggested MIMO antenna was manufactured using a Roger RO6010 substrate and inserted inside a 3D printed flat IMD, as depicted in Fig. 2b. The measurement results for the S-parameters and radiation pattern were achieved employing the setup

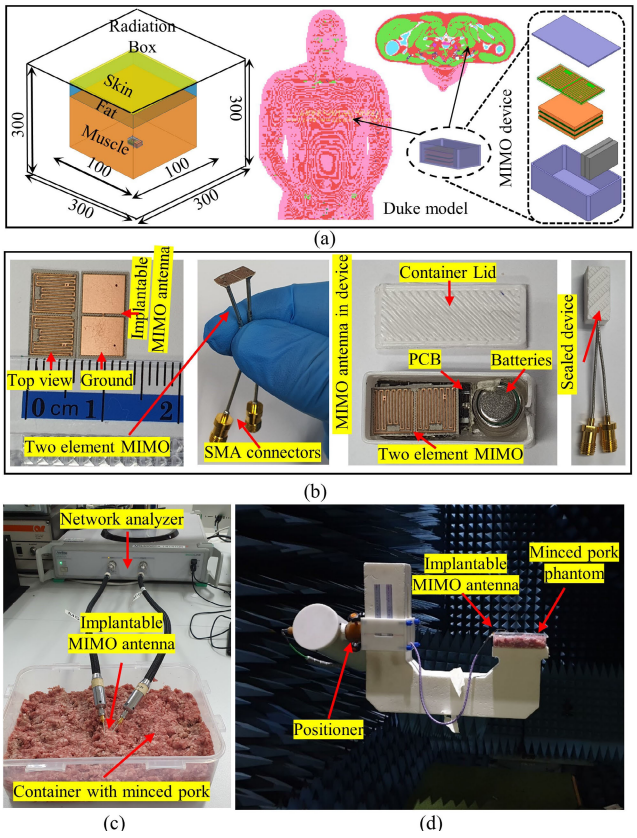

FIGURE 2. (a) Heterogeneous and homogeneous simulation setups, (b) working models of the suggested MIMO antenna and flat IMD, (c) S_{11} measurement in the pork mince, and (d) radiation pattern measurement.

displayed in Figs. 2c and 2d, respectively, by placing the device within the minced pork. The minced pork was employed in the experiment to closely mimic the simulation scenario in which the antenna was implanted in the muscle layer of a multilayer phantom.

The optimization of the suggested MIMO antenna composed of meandered resonators was performed in four steps, as shown in Fig. 3. In step 1, the length of the meandered resonators is determined using (1).

$$L_{MS} = \frac{c}{2 \times f_r \times \sqrt{\varepsilon_r}} \tag{1}$$

$$f_r = \frac{1}{2\pi \times \sqrt{LC}} \tag{2}$$

where L_{MS} is the length of the meandered resonator, c is the velocity of light, f_r is the frequency of operation, ε_r is the permittivity of the substrate, and L and C is the capacitance and inductance, respectively. Two meandered resonators of calculated length were devised, as demonstrated in Fig. 3. The S-parameters (S_{11} and S_{21}) are depicted in Fig. 4, which show that both ports of the proposed MIMO antenna resonate in the 1.76 GHz band with poor impedance matching and a 30 dB isolation between the ports. In step 2, to lower the resonance frequency, the ground plane was trimmed from its center, and slots were added to the patch, resulting in an increased capacitance that shifted the

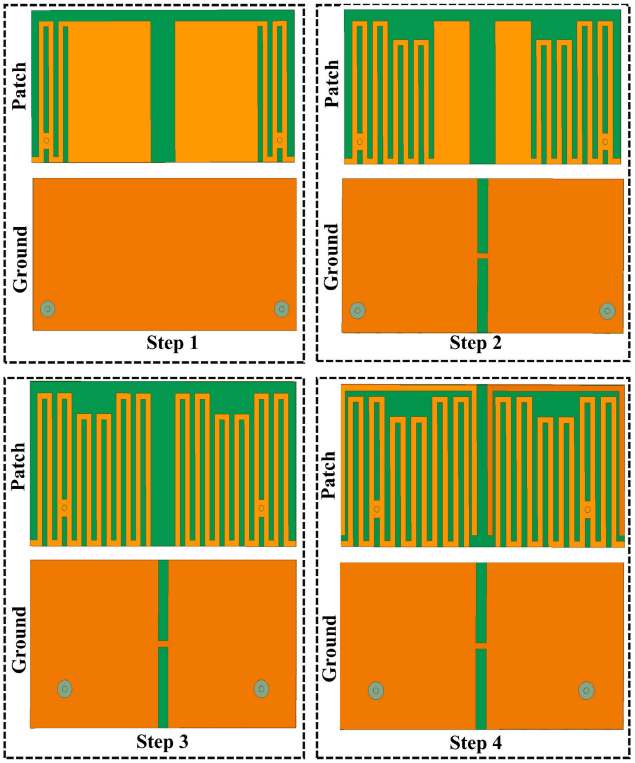

FIGURE 3. Design evolution steps of the proposed MIMO antenna.

resonance frequency (according to (2)) to 940 MHz with poor impedance matching, as depicted in Fig. 4.

Moreover, a second resonance is observed in Fig. 4 at 2120 MHz, with an isolation between the ports at 940 and 2120 MHz of 27 and 30 dB, respectively. In step 3, further slots were added to the patch to adjust the resonances, resulting in the improved matching of the first resonance and a shift in the second resonance to 2550 MHz with almost the same isolation between the ports. In step 4, an outer ring was added to both resonators, shifting the lower resonance to 925 MHz and the upper to 2460 MHz with 27 and 25 dB isolations, respectively. Optimizing the proposed MIMO antenna resulted in dual-band characteristics with improved impedance matching and isolation between the ports, making it a promising solution for multitasking bio-telemetry applications and interference avoidance in deep tissue implants.

III. KEY PARAMETERS ANALYSIS

The effectiveness of the suggested MIMO antenna is dependent upon several parameters. In this section, a parametric analysis has been performed in order to evaluate the suggested antenna's performance pertaining to these parameters. The simulation setup given in Fig.2a (heterogeneous muscle phantom) was used to carry out the parametric analysis. The parameters chosen for the analysis are the feed position and gap relating to the antenna and the electronic elements of the IMD.

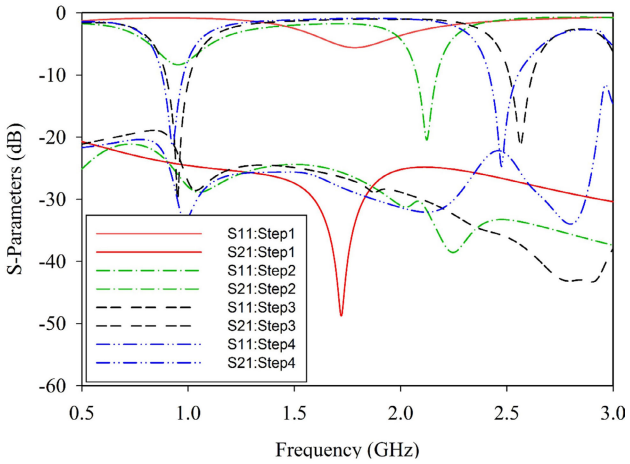

FIGURE 4. S-parameters of the evolution steps.

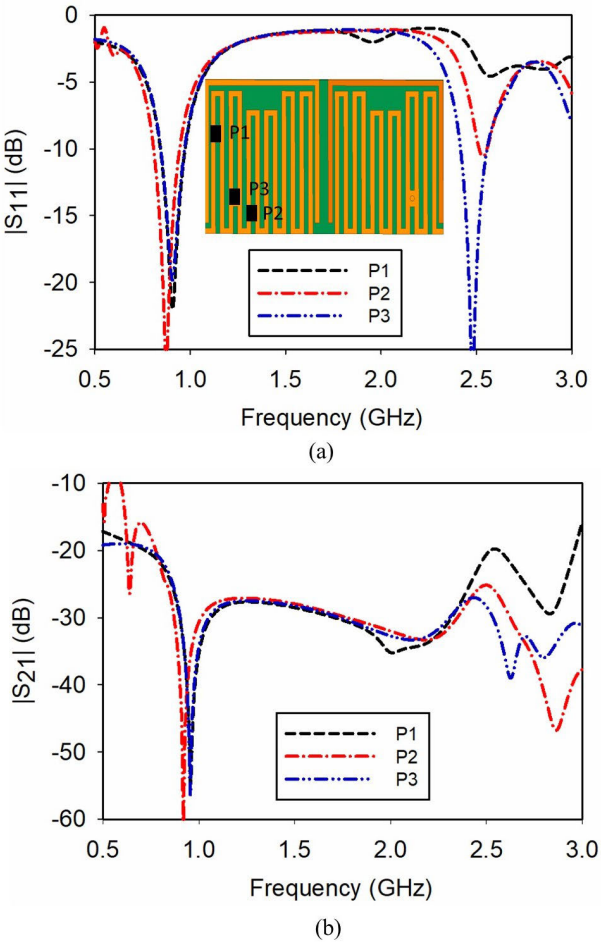

FIGURE 5. Effect of feed position variation on (a) S_{11} and (b) S_{21}.

A. EFFECT OF FEED POSITION

The location of the feeding point plays a significant part in achieving impedance matching at the desirable frequency bands. The proposed MIMO implantable antenna consists of two symmetrical radiating elements; however, this discussion focuses on the results of only one radiating element. The impact of feed position on the S-parameters (S_{11} and S_{21})

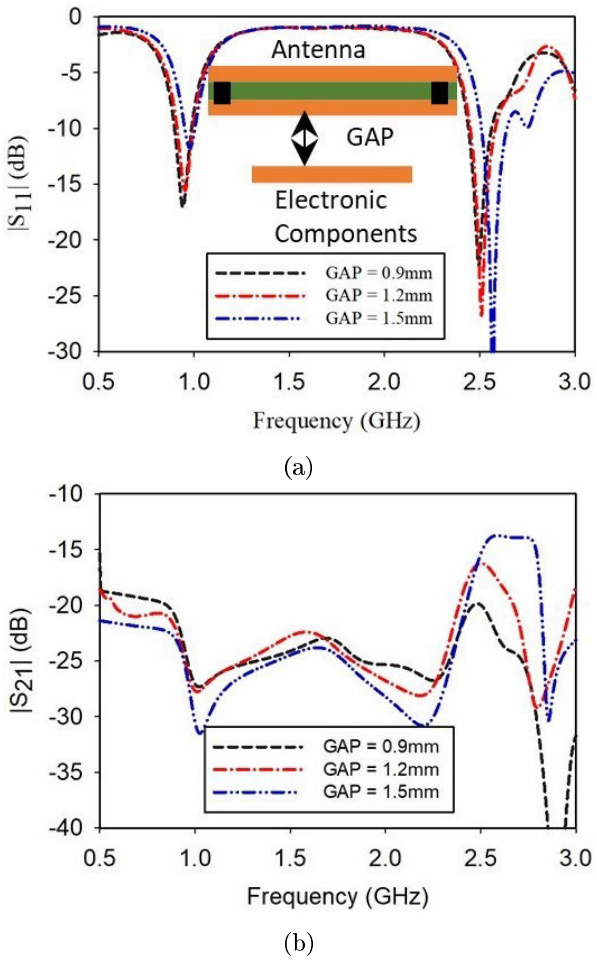

FIGURE 6. Impact of the gap between the antenna and capsule electronics on the antenna performance, including (a) S_{11} and (b) S_{21}.

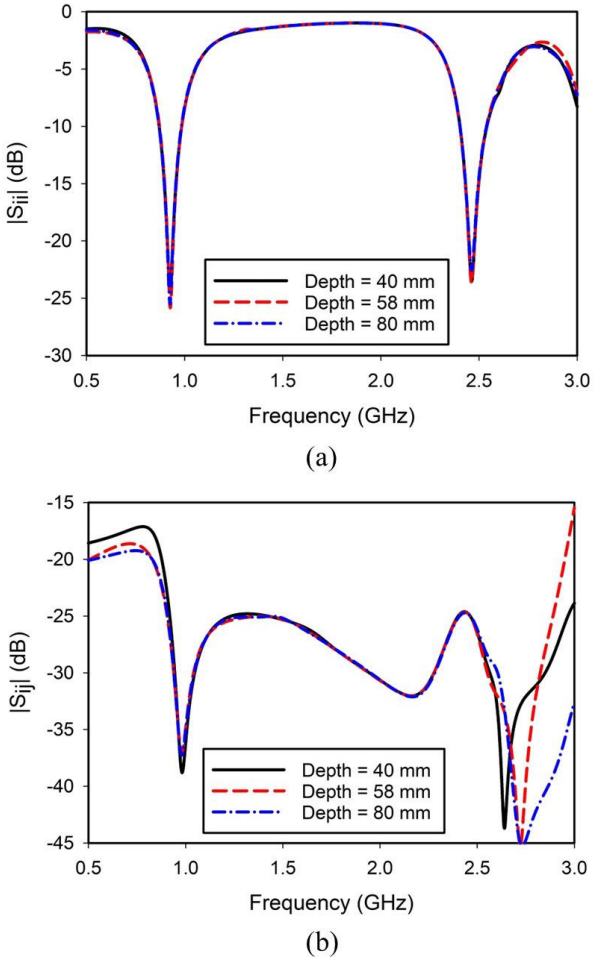

FIGURE 7. Effect of antenna depth on: (a) S_{ii} and (b) S_{ij}.

is shown in Fig. 5a and b. It can be seen in Fig. 5a that variations in feed position have minimal effect on the lower resonance at 915 MHz. However, the impedance of the upper resonance at 2450 MHz is significantly affected by changes in feed position from P1 to P3. At P3, the matching at the first and the second resonances is approximately −22 dB and −25 dB, respectively. Regarding mutual coupling (S_{21}) across the MIMO elements, Fig. 5b demonstrates that it is not significantly influenced by feed position within the band of interest.

B. EFFECT OF ANTENNA PLACEMENT ON COUPLING WITH OTHER ELECTRONIC COMPONENTS

An implantable antenna is a crucial component of an IMD (Implantable Medical Device) that is integrated with other electronic elements such as a camera, LEDs, batteries, and PCB. These parts are placed together along with the antenna (which is usually at the top) in an IMD. Therefore, it is essential to investigate the impact of these components on the antenna's performance. To validate this, a parametric study was performed on the location of the antenna shown as 'Gap' in the inset of Fig. 6a and b. Both the reflection and transmission coefficients are affected by the Gap, as seen in the same figure. It can be examined from Fig. 6a and b that the antenna reflection and transmission coefficients (S_{11} and S_{21}) exhibit minimal dependence on Gap. However, as the Gap increases, the upper resonance at 2450 MHz shifts towards higher frequencies. Optimal results were achieved when the GAP was set to 0.9 mm. Similarly, the variation of GAP has a negligible effect on the mutual coupling (S_{21}) between the antenna elements, as evident from Fig. 6b. The Gap was created by inserting a Styrofoam spacer with a thickness of 0.9 mm and a permittivity close to that of air.

C. EFFECT OF ANTENNA DEPTH ON ANTENNA PERFORMANCE

For the performance evaluation of the proposed antenna with respect to its depth in the phantom a study was conducted and the results are shown in Fig. 7. As clear from Fig. 7a and b the antenna performance (S_{ii} and S_{ij}) remains almost stable in the bands of interest with respect to different depths in the phantom. However, the realized gain of the antenna gets affected as the depth increases. It was noticed that at 915 MHz the gain dropped from −36.07 to −37.2 and then to −41.54 dBi and at 2450 MHz it dropped to −25.58 to

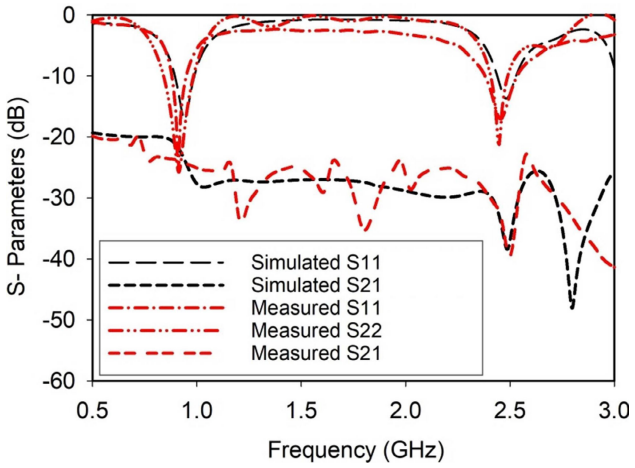

FIGURE 8. Simulated and measured S-parameters.

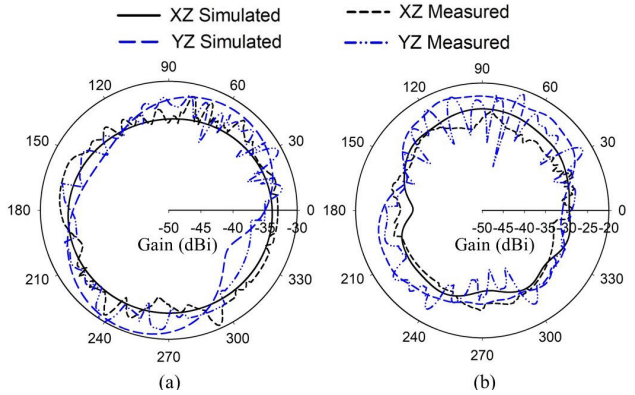

FIGURE 9. Radiation patterns at (a) 915 MHz and (b) 2450 MHz.

−26.41 and then to −29.8 dBi as the depth was increased from 40 mm to 58 mm and then to 80 mm, respectively.

IV. RESULTS AND DISCUSSION

This section presents the results and discussion of the proposed dual-band MIMO antenna. The results are categorized into antenna parameters and MIMO parameters. The antenna characteristics include S-parameters, radiation pattern plots, SAR, and the link budget, while the MIMO parameters encompass envelope correlation coefficient (ECC), diversity gain (DG), total active reflection coefficient (TARC) and channel capacity loss (CCL).

A. ANTENNA PARAMETERS

The suggested implantable MIMO antenna was optimized in homogeneous multi-layer and heterogeneous Duke models. Subsequently, it was integrated with a flat-type IMD for simulation within the same phantoms. The integration of the flat-type IMD with the antenna had minimal impact on its performance, remaining almost unchanged. The antenna was then assembled on a Rogers RO6010 ($\varepsilon_r = 10.2$, $\tan\delta = 0.0023$, and thickness of 0.254 mm) and enclosed in a 3D printed biocompatible alumina-based device, as shown in Fig. 2. Measurements were conducted by placing the device in minced pork meat. To measure the S-parameters

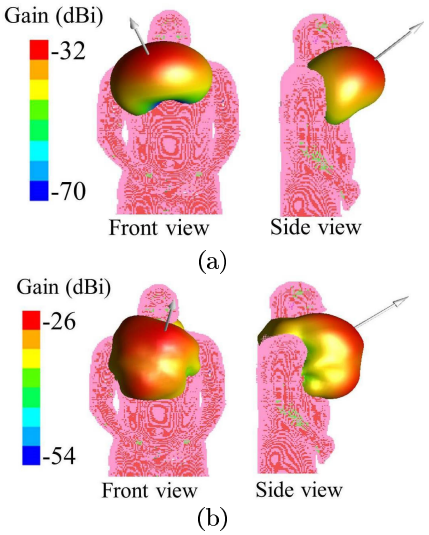

FIGURE 10. 3D radiation patterns of the suggested antenna in the realistic human heart at (a) 915 MHz and (b) 2450 MHz.

of the proposed implantable MIMO antenna, both ports were connected to two ports of a vector network analyzer (VNA). The simulated S-parameter results were then compared with the measured results in Fig. 8. The measured S_{11} and S_{22} exhibited resonances at 915 and 2450 MHz with measured bandwidths of 82.5 MHz (860–942.5 MHz), 148.5 MHz (2379–2527.5 MHz)(port 1) and 130 MHz (840–970 MHz), 89 MHz (2401–2490 MHz) (port 2), respectively. The measured isolation (S_{21}) was greater than 20 and 30 dB at the relevant bands' lower and higher limits.

To further investigate the radiation characteristics of the antenna, radiation pattern measurements were conducted. The radiation patterns were measured by connecting one end of the designed MIMO antenna (serving as the receiving antenna) to the vector network analyzer. In contrast, the other port was matched-terminated with a 50 Ω load in an anechoic chamber. The second port of the VNA was connected to a reference horn antenna, which served as the transmitting antenna. To ensure that the antennas were in the far-field region of each other, the transmitting (Tx) and receiving (Rx) antennas were separated by a distance of 12 m. Fig. 9a-b displays the computed and measured radiation patterns in the 915 and 2450 MHz range in the two major planes (XZ at $\phi = 0°$ and YZ at $\phi = 90°$). At a depth of 58 mm in the muscle phantom, the simulated peak gains for port 1 were −33.2 dBi at 915 MHz and −25.4 dBi at 2450 MHz. The polarization of the antenna remains linear at both the resonance frequency bands. Correspondingly, the measured gains for port 2 were −32.15 dBi at 915 MHz and −22.2 dBi at 2450 MHz. Furthermore, the directivity of the proposed MIMO antenna at 915 and 2450 MHz was computed to be 2.12 and 5.25 dBi, respectively. In addition, antenna performance can be affected by multiple heterogeneous surrounding tissues. As shown in Figures 10a and b, three-dimensional radiation characteristics at 915 and 2450 MHz were studied in a realistic human Duke model using the XFdtd-based simulator Remcom.

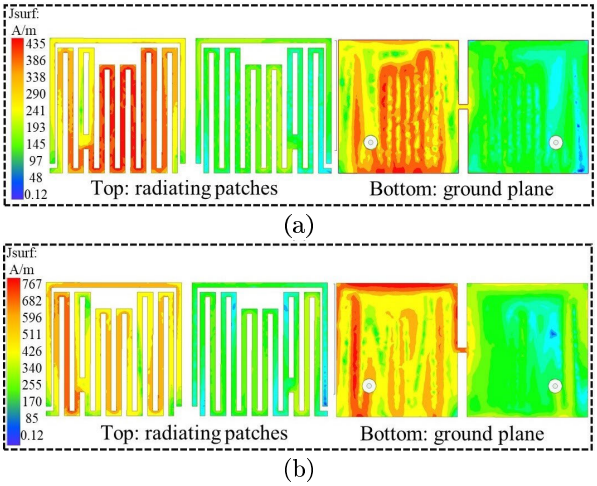

FIGURE 11. Surface current distribution: (a) 915 MHz and (b) 2450 MHz.

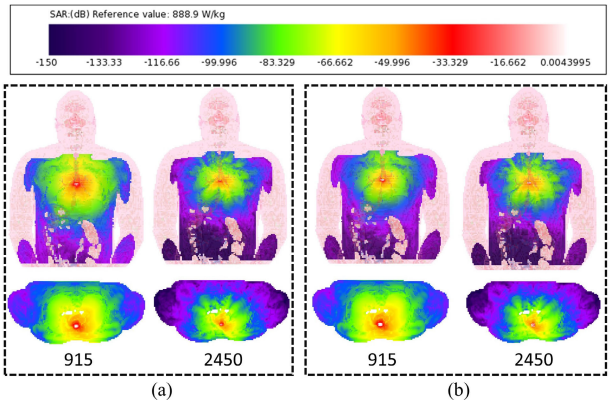

FIGURE 12. SAR distribution at 915 and 2450 MHz ISM band over 1 g of tissue (a) without and (b) with the device when each the ports were fed with 1 W power.

TABLE 1. Analysis of 1g and 10g SAR and maximum allowable power for the proposed MIMO antenna in different scenarios with 1-watt excitation power.

Scenario	Frequency (MHz)	Port Number	1-g SAR (W/kg)	10-g SAR (W/kg)	Maximum allowable power-1-g (mW)	Maximum allowable power-10-g (mW)
Without device	915	P1	888.19	90.57	1.801	22.082
		P2	888.5	90.58	1.800	22.079
	2450	P1	639.31	74.49	2.503	26.851
		P2	622.78	73.99	2.569	27.034
With device	915	P1	813.18	83.44	1.967	23.969
		P2	804.77	83.14	1.988	24.055
	2450	P1	567.13	66.39	2.821	30.125
		P2	594.07	68.75	2.693	29.090

The simulated surface current densities (Js) on the radiating patch and ground plane at both resonance frequencies are shown in Fig. 11. The magnitude Js plots were generated in HFSS by exciting one port and terminating the second with a matched load. Figs. 11a and 12b show the magnitude Js on the patch and ground at 915 and 2450 MHz, respectively. At both resonance frequencies, the maximum Js is concentrated on the excited radiating element with minimum current density leaking towards the unexcited element. A similar behavior is observed for the current density on the ground plane. These results confirm the presence of a high degree of isolation between the two radiating elements of the MIMO system, which is consistent with the isolation (S_{21}) information shown in Fig. 8.

The specific absorption rate (SAR) and the input power are crucial factors for ensuring human safety. Average SAR values over 1 g and 10 g of tissue, respectively, must be less than 1.6 W/kg and 2 W/kg to remain within safe boundaries [10]. To assess the SAR at the desired frequency bands, the suggested MIMO implantable antenna, both with and without device integration, was implanted in the heart muscle of a heterogeneous human Duke model (Remcom), as illustrated in Fig. 2a. Fig. 12 illustrates the 1 g SAR distribution of the proposed MIMO antenna in the heart tissue at 915 MHz and 2450 MHz, with and without the device, for all ports. Table 1 provides the SAR values (1 g and 10 g) for both ports at 915 MHz and 2450 MHz, along with the maximum allowable power. The obtained SAR values with the MIMO antenna embedded inside the device were lower compared to those without the device, primarily due to the use of a biocompatible device made of ceramic alumina material. On the basis of these 1 g SAR values, the utmost permissible power per port (without a device) is 1.8 mW at 915 MHz and 2.5 mW at 2450 MHz. At 915 and 2450 MHz, the utmost permissible power per port (with device) is 1.96 and 2.69 mW, respectively. It should be noted that the maximum allowable power for implantable devices is limited to 25 μW [19], which is significantly lower than the input power of the proposed MIMO antenna. Thus, the proposed antenna can be considered safe for use inside the body.

An implantable antenna plays a crucial role in establishing a reliable wireless link with an external receiver. Therefore, evaluating the link budget is of paramount importance. In this study, the proposed implantable MIMO antenna was placed at a depth of 58 mm, with a gain of −32.15 dBi at 915 MHz and −22.2 dBi at 2450 MHz, acted as the transmitting antenna. Two dipoles resonating at 915 MHz and 2450 MHz, with a gain of 2.15 dBi, served as the receiving antenna. A transmitting power of 25 μW was considered, and the separation (d) between the transmitter and receiver was varied to calculate the resulting link margin. The Friis transmission equation, as provided in [10], was used, taking into account all relevant losses. To validate the real-time data transmission performance of the proposed MIMO implantable antenna we have used software-defined radio modules (NI-USRP2922) to mimic real-time scenarios. The experimental setup shown in Fig. 13a consists of a monopole antenna used as a reference Rx antenna, the proposed MIMO implantable antenna used as a Tx antenna, a Universal Software Radio Peripheral (USRP) device and an ASTM phantom filled with saline solution in which the proposed antenna was

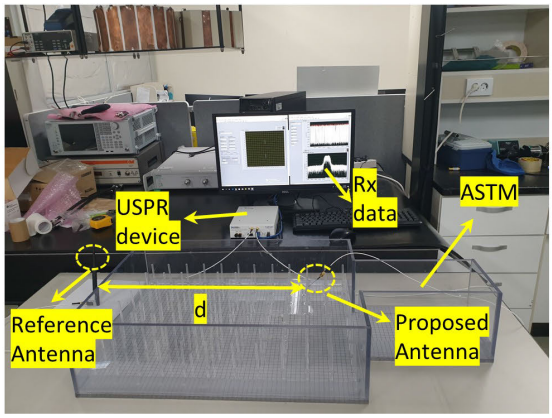

(a)

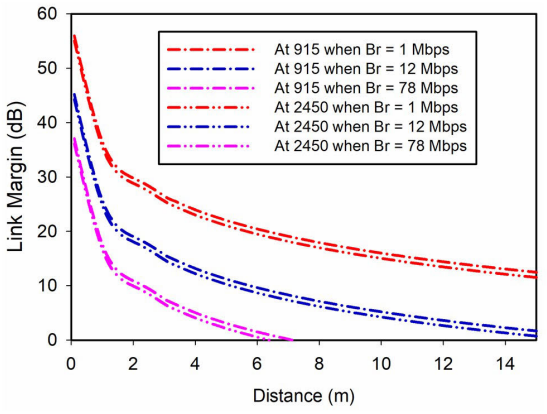

(b)

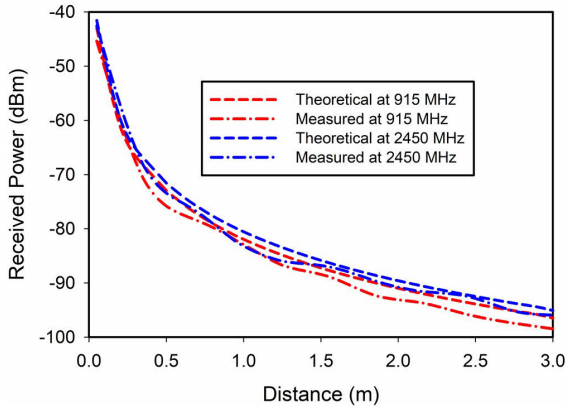

(c)

FIGURE 13. Link margin and received signal strength: (a) Measurement setup, (b) link margin at 915 MHz and 2450 MHz, and (c) received signal measured level at 915 MHz and 2450 MHz.

immersed. For the real-time performance validation, both link margin and received power were calculated. In Fig. 13b, the simulated link margin is assessed at 0 dB across various data rates of 1, 12, and 78 Mbps at the frequency bands of 915 MHz and 2450 MHz. At 915 MHz, the proposed MIMO implantable antenna offers a reliable link for distances exceeding 20 m, 18 m, and 7 m for data rates of 1 Mbps, 12 Mbps, and 78 Mbps, respectively. Similarly, at 2450 MHz, reliable communication is achieved for distances greater than 20 m, 16 m, and 6 m for data rates of 1 Mbps, 12 Mbps, and 78 Mbps, respectively. Similarly, Fig. 13c shows the received signal measured level when received by an external antenna for a varying distance (d) between 0.05 - 3 m within an indoor propagation environment. During the experiment, a quadrature phase shift keying (QPSK) modulation scheme was employed, accompanied by a sampling rate of 500 ksamples/sec and a Tx power of −16 dBm (25 μW). Each data packet contained eight samples per symbol. As evident from Fig. 13c, at both operating frequencies (915 MHz and 2450 MHz) and distances of up to 3 m, the theoretically predicted and measured received power levels exceeding −100 dBm exhibit a close match. However, slight deviations between theoretical and measured results could be attributed to environmental losses.

B. MIMO PARAMETERS

For the designed MIMO antenna, it is important to calculate the different antenna parameters, such as the reflection coefficient, gain, and current distribution, as well as MIMO and diversity parameters including the envelope correlation coefficient (ECC), diversity gain (DG), total active reflection coefficient (TARC) and capacity loss (CL). The ECC evaluates the interdependence of the MIMO elements, and its ideal value is zero, which implies that the MIMO elements are completely independent. However, an ECC value below 0.5 is generally considered acceptable [23], [25]. The ECC was computed utilizing the far-field radiation patterns of the suggested MIMO antenna, as expressed by the expression (3).

$$ECC = \frac{|\iint_0^{4\pi}[\vec{A}_i(\theta,\phi) \times \vec{A}_j(\theta,\phi)d\Omega]|^2}{\iint_0^{4\pi}|\vec{A}_i(\theta,\phi)|^2 d\Omega \iint_0^{4\pi}|\vec{A}_j(\theta,\phi)|^2 d\Omega} \quad (3)$$

where $\vec{A}_i$ (θ, ϕ) and $\vec{A}_j$ (θ, ϕ) represent the 3D patterns of the ith and jth antenna parts, respectively, and Ω denotes the solid angle. The ECC values of the proposed MIMO antenna in the relevant bands are less than 0.25, as shown in Fig. 14a and 14b.

Similarly, DG serves as another important MIMO performance parameter, quantifying the reduction in transmitted power when implementing a diversity scheme with any associated loss in antenna performance. DG is calculated using the following equation [19]:

$$DG = 10\sqrt{1 - (ECC)^2} \quad (4)$$

For an uncorrelated channel, the value of DG is 10 dB in the ideal case. The value of DG for the proposed MIMO antenna in the relevant bands was 9.6 dB, as shown in Fig. 14.

TARC is defined as the ratio of the square root of the total incident power to the reflected power in a MIMO system. It is used to account for the effect on the performance of a MIMO antenna when the antenna elements operate concurrently in a multiport system like a MIMO. For a two-port MIMO system

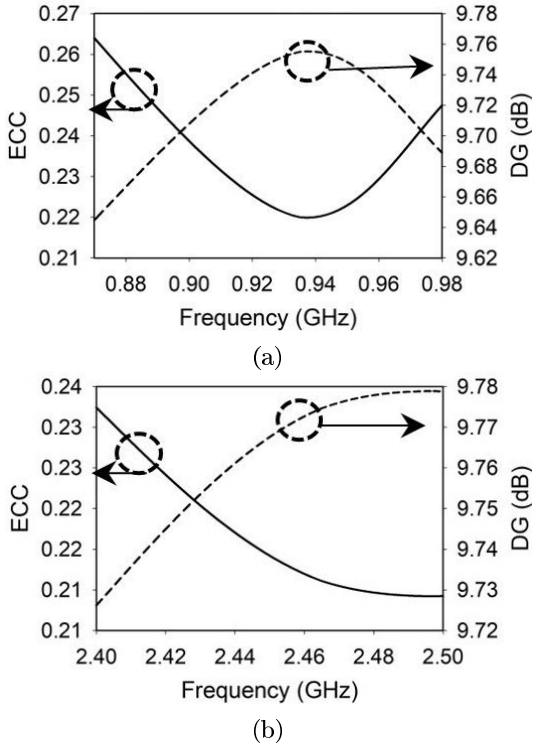

FIGURE 14. ECC and DG at (a) at 915 MHz and (b) 2450 MHz.

like the proposed design, TARC can be computed as [30]:

$$TARC = \frac{\sqrt{(S_{11} + S_{22})^2 + (S_{21} + S_{12})^2}}{\sqrt{2}} \quad (5)$$

The TARC of the proposed MIMO antenna is depicted in Fig. 15a, illustrating various phase variations in the input signal. Notably, the bandwidth and resonant frequencies exhibit negligible changes, remaining relatively constant and thereby ensuring robust MIMO performance. Similarly, CCL gives the ultimate cut-off on the data transmission rate over the transmission channel and is given as [30]:

$$C(loss) = -\log_2 det(\alpha^R) \quad (6)$$

where $\alpha^R = \begin{bmatrix} R_{11} & R_{12} \\ R_{21} & R_{22} \end{bmatrix}$, $R_{ii} = 1 - (|S_{11}|^2 + |S_{22}|^2)$ and $R_{ij} = -(S_{ii}^* S_{ij} + S_{ji}^* S_{jj})$ for $i, j = 1$ or 2.

The CCL of the proposed MIMO implantable antenna is presented in Fig. 15b. Within the bands of interest, the CCL remains below 0.1 b/sec/Hz, which is notably lower than the established standard of 0.4 b/s/Hz [30].

The performance of the proposed dual-band implantable MIMO antenna is compared with that of other MIMO implantable antennas available in the literature, as presented in Table 2. The implantable MIMO antennas listed in Table 2 have only single-band characteristics. By contrast, the proposed work has dual-band capabilities, which, to the authors' knowledge, is a first-of-its-kind design for deep-tissue applications. Moreover, the proposed MIMO implantable antenna demonstrates potential as a promising solution for deep-tissue biomedical applications owing to its dual-band capabilities for interference avoidance, larger implant depth, low ECC, high DG, acceptable TARC and CCL making it well suited to meet the demands of deep-tissue communication.

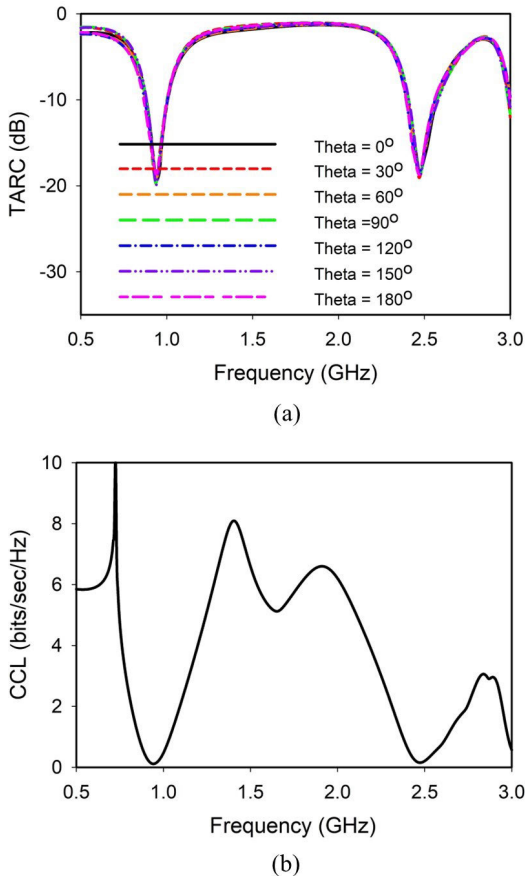

FIGURE 15. (a) TARC and (b) CCL.

TABLE 2. Comprehensive comparison of proposed MIMO antenna with current state-of-the-art solutions.

Reference	[19]	[23]	[24]	[27]	[28]	Proposed work
Size volume (λg^3)	0.139×0.161 × 0.0031	0.3×0.15 × 0.002	0.048×0.048 × 0.003	0.13×0.109 × 0.003	0.2 × 0.399 × 0.024	0.105 × 0.054 × 0.0024
Frequency (MHz)	2450	915	2450	2450	2400	915, 2450
Bandwidth (%)	13	14	18.64	25.2	8.5	9,6
Isolation (dB)	>28	10	>15.9	30.1	37	>24
Single / dual-band	Single-band	Single-band	Single-band	Single-band	Single-band	Dual-band
Implant depth (mm)	75	65	4	80	3	58
Number of elements	2	4	4	2	2	2
ECC	<0.1	<0.4	0.0025	<0.11	--	<0.2
DG (dB)	9.98	9	--	9.9	--	>9.96
Antenna type	Meandered	Meandered	EBG	Meandered	Patch	Meandered

V. CONCLUSION

We have proposed a compact, dual-band, two-port MIMO implantable antenna designed for high-speed data transmission in deep tissues. The MIMO antenna operates in the 915 and 2450 MHz ISM bands, offering a measured bandwidth of 82.5 MHz (port 1) and 148.5 MHz, as well as peak gains of -32.15 and -22.2 dBi, respectively. The compact dimensions of $10.8 \times 5.6 \times 0.254$ mm^3 for the MIMO antenna are achieved by using meandered resonators and two slots on the ground plane. This configuration has also provided excellent port isolation. To validate the performance of the MIMO antenna system, experiments were conducted in minced pork, and the obtained results closely align with the simulation data. Furthermore, the MIMO performance parameters, namely ECC and DG, have been calculated and demonstrate satisfactory outcomes. The developed antenna shows great potential for facilitating effective communication within the human body for various deep-tissue biomedical applications based on favorable results from both simulations and measurements.

To enhance the performance of the proposed MIMO implantable antenna for future applications, one potential solution is to increase the number of ports, which would enhance channel capacity and overall efficiency. Given the relatively compact size of the antenna, incorporating additional ports, such as two more, remains feasible without compromising its suitability for implantable use. Additionally, for some future biotelemetry applications, a reduction in antenna size can be pursued by incorporating shorting vias or patch stacking. The vias effectively integrate the ground plane with the radiating structure, thereby elongating the effective current path and resulting in lower resonance frequencies. However, it's important to acknowledge that these approaches introduce complexity in design and fabrication.

ACKNOWLEDGMENT

(Syed Nazim Shah and Muhammad Zada are co-first authors.)

REFERENCES

[1] A. Basir and H. Yoo, "A stable impedance-matched ultrawideband antenna system mitigating detuning effects for multiple biotelemetric applications," *IEEE Trans. Antennas Propag.*, vol. 67, no. 5, pp. 3416–3421, May 2019.

[2] M. Zada, I. A. Shah, A. Basir, and H. Yoo, "Ultra-compact implantable antenna with enhanced performance for leadless cardiac pacemaker system," *IEEE Trans. Antennas Propag.*, vol. 69, no. 2, pp. 1152–1157, Feb. 2021.

[3] B. Lee, M. K. Koripalli, Y. Jia, J. Acosta, M. S. E. Sendi, Y. Choi, and M. Ghovanloo, "An implantable peripheral nerve recording and stimulation system for experiments on freely moving animal subjects," *Sci. Rep.*, vol. 8, no. 1, p. 6115, Apr. 2018.

[4] S. Hayat, S. A. A. Shah, and H. Yoo, "Miniaturized dual-band circularly polarized implantable antenna for capsule endoscopic system," *IEEE Trans. Antennas Propag.*, vol. 69, no. 4, pp. 1885–1895, Apr. 2021.

[5] R. Das and H. Yoo, "A wideband circularly polarized conformal endoscopic antenna system for high-speed data transfer," *IEEE Trans. Antennas Propag.*, vol. 65, no. 6, pp. 2816–2826, Jun. 2017.

[6] J.-C. Chiou, S.-H. Hsu, Y.-T. Liao, Y.-C. Huang, G.-T. Yeh, C.-K. Kuei, and K.-S. Dai, "Toward a wirelessly powered on-lens intraocular pressure monitoring system," *IEEE J. Biomed. Health Informat.*, vol. 20, no. 5, pp. 1216–1224, Sep. 2016.

[7] X. Y. Liu, Z. T. Wu, Y. Fan, and E. M. Tentzeris, "A miniaturized CSRR loaded wide-beamwidth circularly polarized implantable antenna for subcutaneous real-time glucose monitoring," *IEEE Antennas Wireless Propag. Lett.*, vol. 16, pp. 577–580, 2017.

[8] A. Basir, M. Zada, Y. Cho, and H. Yoo, "A dual-circular-polarized endoscopic antenna with wideband characteristics and wireless biotelemetric link characterization," *IEEE Trans. Antennas Propag.*, vol. 68, no. 10, pp. 6953–6963, Oct. 2020.

[9] A. Kiourti and K. S. Nikita, "Miniature scalp-implantable antennas for telemetry in the MICS and ISM bands: Design, safety considerations and link budget analysis," *IEEE Trans. Antennas Propag.*, vol. 60, no. 8, pp. 3568–3575, Aug. 2012.

[10] S. M. A. Shah, M. Zada, J. Nasir, and H. Yoo, "Ultraminiaturized triband antenna with reduced SAR for skin and deep tissue implants," *IEEE Trans. Antennas Propag.*, vol. 70, no. 9, pp. 8518–8529, Sep. 2022.

[11] R. Das and H. Yoo, "A multiband antenna associating wireless monitoring and nonleaky wireless power transfer system for biomedical implants," *IEEE Trans. Microw. Theory Techn.*, vol. 65, no. 7, pp. 2485–2495, Jul. 2017.

[12] A. Basir and H. Yoo, "Efficient wireless power transfer system with a miniaturized quad-band implantable antenna for deep-body multitasking implants," *IEEE Trans. Microw. Theory Techn.*, vol. 68, no. 5, pp. 1943–1953, May 2020.

[13] L. V. Tung and C. Seo, "A miniaturized implantable antenna for wireless power transfer and communication in biomedical applications," *J. Electromagn. Eng. Sci.*, vol. 22, no. 4, pp. 440–446, Jul. 2022.

[14] M. Zada and H. Yoo, "Miniaturized dual band antennas for intra-oral tongue drive system in the ISM bands 433 MHz and 915 MHz: Design, safety, and link budget considerations," *IEEE Trans. Antennas Propag.*, vol. 67, no. 9, pp. 5843–5852, Sep. 2019.

[15] L.-J. Xu, Y. Bo, W.-J. Lu, L. Zhu, and C.-F. Guo, "Circularly polarized annular ring antenna with wide axial-ratio bandwidth for biomedical applications," *IEEE Access*, vol. 7, pp. 59999–60009, 2019.

[16] K. Zhang, C. Liu, X. Liu, H. Guo, and X. Yang, "Miniaturized circularly polarized implantable antenna for ISM-band biomedical devices," *Int. J. Antennas Propag.*, vol. 2017, pp. 1–9, Mar. 2017.

[17] A. Basir, M. Zada, and H. Yoo, "Compact and flexible wideband antenna for intraoral tongue-drive system for people with disabilities," *IEEE Trans. Antennas Propag.*, vol. 68, no. 3, pp. 2405–2409, Mar. 2020.

[18] Z. Xia, H. Li, Z. Lee, S. Xiao, W. Shao, X. Ding, and X. Yang, "A wideband circularly polarized implantable patch antenna for ISM band biomedical applications," *IEEE Trans. Antennas Propag.*, vol. 68, no. 3, pp. 2399–2404, Mar. 2020.

[19] A. J. Alazemi and A. Iqbal, "A high data rate implantable MIMO antenna for deep implanted biomedical devices," *IEEE Trans. Antennas Propag.*, vol. 70, no. 2, pp. 998–1007, Feb. 2022.

[20] P. L. Poshtgol, L. Jichao, S. Soltani, and R. D. Murch, "MIMO antennas for capsule endoscope systems," in *Proc. IEEE Int. Symp. Antennas Propag. (APSURSI)*, Jun. 2016, pp. 1175–1176.

[21] L. Xu, B. Li, M. Zhang, and Y. Bo, "Conformal MIMO loop antenna for ingestible capsule applications," *Electron. Lett.*, vol. 53, no. 23, pp. 1506–1508, Nov. 2017.

[22] A. Iqbal, M. Al-Hasan, I. B. Mabrouk, and M. Nedil, "A compact implantable MIMO antenna for high-data-rate biotelemetry applications," *IEEE Trans. Antennas Propag.*, vol. 70, no. 1, pp. 631–640, Jan. 2022.

[23] Y. Wang, B. Huang, and S. Yan, "A conformal four-antenna module for capsule endoscope MIMO operation," *IEEE Trans. Antennas Propag.*, vol. 70, no. 11, pp. 10270–10285, Nov. 2022.

[24] Y. Fan, J. Huang, T. Chang, and X. Liu, "A miniaturized four-element MIMO antenna with EBG for implantable medical devices," *IEEE J. Electromagn., RF Microw. Med. Biol.*, vol. 2, no. 4, pp. 226–233, Dec. 2018.

[25] A. Iqbal, M. Al-Hasan, I. B. Mabrouk, and M. Nedil, "Scalp-implantable MIMO antenna for high-data-rate head implants," *IEEE Antennas Wireless Propag. Lett.*, vol. 20, no. 12, pp. 2529–2533, Dec. 2021.

[26] B. Biswas, A. Karmakar, and V. Chandra, "Hilbert curve inspired miniaturized MIMO antenna for wireless capsule endoscopy," *AEU Int. J. Electron. Commun.*, vol. 137, Jul. 2021, Art. no. 153819.

[27] A. J. Alazemi and A. Iqbal, "A compact and wideband MIMO antenna for high-data-rate biomedical ingestible capsules," *Sci. Rep.*, vol. 12, no. 1, p. 14290, Aug. 2022.

[28] M. S. Singh, J. Ghosh, S. Ghosh, and A. Sarkhel, "Miniaturized dual-antenna system for implantable biotelemetry application," *IEEE Antennas Wireless Propag. Lett.*, vol. 20, no. 8, pp. 1394–1398, Aug. 2021.
[29] F. Kong, M. Zada, H. Yoo, and M. Ghovanloo, "Adaptive matching transmitter with dual-band antenna for intraoral tongue drive system," *IEEE Trans. Biomed. Circuits Syst.*, vol. 12, no. 6, pp. 1279–1288, Dec. 2018.
[30] S. Kumar, D. Nandan, K. Srivastava, S. Kumar, H. Singh, M. Marey, H. Mostafa, and B. K. Kanaujia, "Wideband circularly polarized textile MIMO antenna for wearable applications," *IEEE Access*, vol. 9, pp. 108601–108613, 2021.

SYED NAZIM SHAH received the B.Sc. degree in telecommunication engineering from the University of Engineering and Technology, Peshawar, Pakistan, in 2016, and the M.S. degree in electrical engineering from the Department of Electrical Engineering, COMSATS University Islamabad, Abbottabad Campus, Pakistan, in 2021. His research interests include slotted waveguide arrays, machine-learning assisted antennas, reflectarrays, implantable antennas, MIMO antennas, dielectric resonator antennas, wireless power transfer, and synthesis of magnetoelectric dipole antennas.

MUHAMMAD ZADA (Graduate Student Member, IEEE) received the B.Sc. degree in telecommunication engineering from the University of Engineering and Technology, Peshawar, Pakistan, in 2015, and the integrated M.S./Ph.D. degrees in electronic engineering from Hanyang University, Seoul, South Korea, in 2023.

He is currently a Postdoctoral Fellow with Hanyang University, where he conducts research in the field of electronic and biomedical engineering. He has published several papers in high-quality international journals and conference proceedings. His current research interests include implantable antennas and devices, intra-oral tongue drive systems, wireless power transfer, energy harvesting, smart-textile, millimeter-wave antennas, MIMO antennas, frequency and pattern reconfigurable antennas, wearable sensors and antennas, microwave breast cancer detection, metamaterials, and electromagnetic bandgap structures.

Dr. Zada received the Best Student Paper Competition 2018 Award from the Korean Institute of Electromagnetic Engineering and Science (KIEES). He is serving as a Reviewer for several IEEE Transactions, the *International Journal of RF and Microwave Computer-Aided Engineering* (RFCAD), and Elsevier journals.

JAMAL NASIR was born in Khyber Pakhtunkhwa, Pakistan. He received the M.Sc. degree in mobile and satellite communication from the University of Bradford, U.K., in 2007, and the Ph.D. degree in electrical engineering from Universiti Technologi Malaysia, in 2017. He is currently an Assistant Professor with the Department of Electrical and Computer Engineering, COMSATS University Islamabad, Abbottabad Campus, Khyber Pakhtunkhwa. His research interests include SIW-based passive components and antenna arrays, meta-materials-based antenna and microwave components, phased arrays and smart antennas, mutual coupling analysis and compensation in phased and smart antenna arrays, MIMO antennas, massive MIMO, dielectric resonator antennas, UWB antennas, slotted waveguide arrays, ingestible and implantable antennas, and wearable antennas.

SYED MANAF ALI SHAH received the degree in telecommunication from Hazara University, Dhodial, Mansehra, Pakistan, in 2016, and the M.S. degree in electrical engineering from the Department of Electrical Engineering, COMSATS University Islamabad, Abbottabad, Pakistan, in 2021. His research interests include printed antennas, flexible antennas, implantable antennas, MIMO antennas, dielectric resonator antennas, wireless power transfer, and synthesis of microwave components.

EMILIO ARNIERI (Member, IEEE) was born in Cosenza, Italy, in 1977. He received the degree (Hons.) in information technology engineering from the University of Calabria, Rende, Italy, in 2003, and the Ph.D. degree in electronics engineering from the University Mediterranea of Reggio Calabria, Reggio Calabria, Italy, in 2007. He is currently an Assistant Professor with the Department of Informatics, Modeling, Electronics and System Engineering, University of Calabria, where he has participated in several national, EU, and ESA projects. He is the co-founder of the academic Spin-off. He has coauthored more than 70 articles published in international journals and proceedings of international conferences. His current research interests include circular polarizers, the development of dual-band antennas and millimeter-wave components, synthetic aperture radar, and beam scanning antennas. He was selected as a finalist for the Best Paper Award in Antenna Design at the 13th European Conference on Antennas and Propagation (EuCap 2019). He serves as an Associate Editor for the IEEE Antennas and Wireless Propagation Letters and an Advisory Editor for the *Engineering Reports* (Wiley).

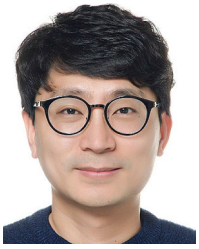

HYOUNGSUK YOO (Senior Member, IEEE) received the B.Sc. degree in electrical engineering from Kyungpook National University, Daegu, South Korea, in 2003, and the M.Sc. and Ph.D. degrees in electrical engineering from the University of Minnesota, Minneapolis, MN, USA, in 2006 and 2009, respectively.

In 2009, he joined the Center for Magnetic Resonance Research, University of Minnesota, as a Postdoctoral Associate. In 2010, he joined Cardiac Rhythm Disease Management, Medtronic, MN, as a Senior EM/MRI Scientist. From 2011 to 2018, he was an Associate Professor with the Department of Biomedical Engineering, School of Electrical Engineering, University of Ulsan, Ulsan, South Korea. Since 2018, he has been a Full Professor with the Department of Biomedical Engineering and the Department of Electronic Engineering, Hanyang University, Seoul, South Korea. He has been the CEO of E2MR, Seoul, a startup company, since 2017. His current research interests include electromagnetic theory, numerical methods in electromagnetics, metamaterials, antennas, implantable devices, and magnetic resonance imaging in high-magnetic field systems.

Dr. Yoo received the Third Prize of the Best Student Paper at the 2010 IEEE Microwave Theory and Techniques Society International Microwave Symposium.